Journal Name

ARTICLE

Progress in fabrication of long transparent YAG:Ce and YAG:Ce,Mg single crystalline fibers for HEP applications

Received 00th January 20xx,
Accepted 00th January 20xx

DOI: 10.1039/x0xx00000x

www.rsc.org/

O. Sidletskiy[a,*], K. Lebbou[b], D. Kofanov[a], V. Kononets[a], Ia. Gerasymov[a], R. Bouaita[b], V. Jary[c], R. Kucerkova[c], M. Nikl[c], A. Polesel[d], K. Pauwels[d,e], E. Auffray[d]

A significant enhancement in the light attenuation length in 22 cm long YAG:Ce and YAG:Ce,Mg fibers grown by the micro-pulling-down method has been reported. This has been achieved by the introduction of Al excess into the melt, optimization of thermal conditions of crystallization and post growth annealing. Attenuation length clearly correlates with surface roughness of the fibers. Al excess addition over the stoichiometric composition enhances the fiber surface smoothness. Increase of axial thermal gradient and melt pressure in the crucible capillary die improves the crystallization process stability. Mg codoping provides the Ce^{3+} scintillation decay time decrease down to 80 ns.

1. Introduction

Single crystalline fibers are considered as one of alternatives capable to substitute bulk scintillators at future collider experiments. For instance, a feasibility of dual registration of Cherenkov and scintillation light by undoped and Ce-doped LuAG fibers, correspondingly, was shown [1]. Long >20 cm fibers with a good transparency (attenuation length L_{att} > 40 cm) are needed to minimize light losses [1]. Different methods to obtain garnet fibers with the required parameters have been under discussion, for instance, cutting bulk crystals [2] obtained by the Czochralski method. Despite a good transparency and radiation hardness [2] of garnet fibers cut from bulk crystal, micro-pulling-down (μ-PD) is still the only method to produce >20 cm long fibers of needed shape without cutting and additional crystal treatment [3]. Previously we reported the obtaining of LuAG:Ce fibers with the length over 22 cm and excellent transparency (attenuation length L_{att} of up to 104 cm) [4]. Further efforts have been focused at YAG:Ce fibers as a low-cost alternative to LuAG:Ce due to cheaper starting materials. Meanwhile, L_{att} of YAG:Ce was much worse compared to LuAG:Ce and not exceeded 18 cm [3]. The attenuation length degraded down to 12 cm in YAG:Ce fibers codoped with Mg^{2+} for acceleration of Ce^{3+} luminescence decay [3].

Transparency degradation in some LuAG:Ce fibers was linked to scattering centers created on inclusions consisting of microscopic gas bubbles [5]. Inclusions are formed at deterioration of steady-state conditions of crystallization, namely variation of melt meniscus thickness and shape during μ-PD growth. Segregation of Ce^{3+} activator and admixtures to the fiber periphery is another cause of unstable fiber growth leading to roughness of fiber surface. The latter impedes light propagation along the fibers.

Also, garnet crystals contain several types of point defects responsible for color centers formation calling additional absorption in UV- and visible bands. They comprise oxygen and Al^{3+} vacancies, as well as various complex defects, for example $Lu(Y)_{Al}$ antisite defects, see for ex., the review [6]). A high concentration of oxygen vacancies in as-grown garnet fibers has been evidenced by a drastic enhancement of LuAG:Ce fiber transmission after thermal annealing in air [4]. Al and Al-O vacancies in YAG evidenced by positron annihilation spectroscopy [7] may be responsible as well for deterioration of optical and scintillation parameters. Previously we reported a strong depletion of YAG crystal surface layer with oxygen and aluminum at Czochralski growth and post-growth annealing due to crystal surface interaction with reducing Ar+CO atmosphere [8]. Though YAG:Ce fibers in the present work are grown under weakly oxidizing atmosphere conditions (Ar with low amount of oxygen), the depletion of melt and fiber surface with these ions is also possible keeping in mind the melt overheating in μ-PD method, as well as flowing Ar gas atmosphere.

[a] Institute for Scintillation Materials NAS of Ukraine, 60 Nauky Ave., 61072, Kharkiv, Ukraine
[b] Institut Lumière Matière UMR 5306, Université Lyon, Université Claude Bernard Lyon 1, CNRS, 69100, Villeurbanne, France
[c] Institute of Physics, Academy of Sciences of Czech Republic, Cukrovarnicka str., 10, 16200 Prague, Czech Republic
[d] European Organization for Nuclear Research, Geneva 23, Switzerland
[e] European Synchrotron Radiation Facility, 71, avenue des Martyrs, 38043 Grenoble, France

* Corresponding author

This paper reports the progress on the transmission of 22-55 cm long YAG:Ce and YAG:Ce,Mg fibers growth by the μ-PD method. Post growth annealing in air atmosphere and addition of Al^{3+} excess into the melt over the stoichiometric composition have been used to compensate oxygen and Al vacancies formed due to evaporation of Al_2O_3 and its components. Thermal conditions of crystallization were modified to achieve a better stability of growth process and to reduce the amount of scattering centers in fibers.

2. Experimental

2.1 Raw material preparation and fabrication of fiber samples for measurements

YAG:Ce fibers were grown from the melt by the micro-pulling down (μ-PD) technique. All experiments were carried out using Ir crucible and afterheater in inert Ar atmosphere. Chunks of undoped and 0.1% Ce-doped YAG crystals grown by the Czochralski method at Crytur (Czech Republic) and ISMA (Ukraine) were used as the raw materials. The concentration of Ce in the melt varied within the 100-200 ppm range. Magnesium with the concentration of up to 40 ppm was introduced in the form of MgO (purity 99.95%) or $MgCO_3$ ("pure for analysis") powders. Obtained fibers were ~ 2.0 - 2.2 mm dia., similar to the diameter of the crucible capillary die. The fibers were grown with the rates of 0.2-0.3 mm/min on YAG:Ce seeds with the [521] orientation. The lengths of grown fibers were 25 – 55 cm. Then the fibers were cut into the 22 cm long samples (for attenuation length measurement) and ~1 cm long samples for scintillation decay time measurements.

2.2 Attenuation length measurements

Attenuation length was taken as the main indicator of optical quality of fibers. The measurements were performed by illuminating the fibers with a 470 nm pulsed LED beam focused on the periphery of fiber, moving the LED at constant speed along fiber longitudinal axis, and monitoring the luminescence output through dry coupling both fiber ends to two Hamamatsu H6610 photomultiplier tubes (PMT) working at 2 kV. Long-pass filters (ThorLabs FGL420) were used to avoid parasitic excitation light. Signals were then acquired with a digitizer (Model DT5720 from CAEN), see the details in [9].

2.3 Scintillation decay time determination

Scintillation decay measurements were performed by coupling the crystals to a Hamamatsu R375 PMT and under excitation with 662 keV γ-rays from a ^{137}Cs source. Scintillation decay curves were recorded using Tektronix TDS 3052C digital oscilloscope. Convolution procedure was applied to the decay curves to determine true decay times (SpectraSolve software package, Ames Photonics).

2.4 EPMA measurements

The longitudinal distributions of the Ce concentration in the grown fibers were analyzed using electron probe microanalysis (EPMA), JEOL JXA-8621MX by bombarding a micro-volume of a fiber with a focused electron beam (energy = 15 keV). It is quantitative method of micron-sized volumes at the surface of materials, with sensitivity at the level of ppm.

3. Results and discussion

3.1 Condition of the fiber surface and Al deficiency in the melt

Analyzing the surface of fibers with large and small attenuation lengths obtained in the prior and current works, we noticed that the fiber surface roughness clearly correlates with the attenuation length degradation in fibers. One may see (Fig. 1) that the surface of LuAG:Ce fiber with the excellent L_{att} is very smooth (Fig. 1a), contrary to the wavy defects observed at the surface of LuAG:Ce fiber with low L_{att}. (Fig. 1b). These periodical "waves" oriented perpendicular to the growth direction are formed after variation of melt meniscus shape, evidently, due to constitutional supercooling at the crystallization interface and/or instable thermal conditions. Similar tendency is observed in YAG:Ce fibers: the surface of YCV30 fiber with a high L_{att} was rather smooth, while some grooves could be noticed in the tail part of the same fiber with bad transparency (Fig. 1c,d). Variation of fiber diameter can be related both to Ce segregation to the fiber periphery [5] and by Al deficiency in the melt, as well as by unstable thermal conditions of the crystallization. Microscopic observations also show the presence of gas bubbles in both LuAG:Ce and YAG:Ce fibers (Fig. 1a,c,d) – in Fig. 1c they are aligned along the growth direction. However, the presence of gas bubbles in fibers with both low and high attenuation lengths certifies that bubbles have a minor impact on L_{att} of fibers compared to the surface roughness.

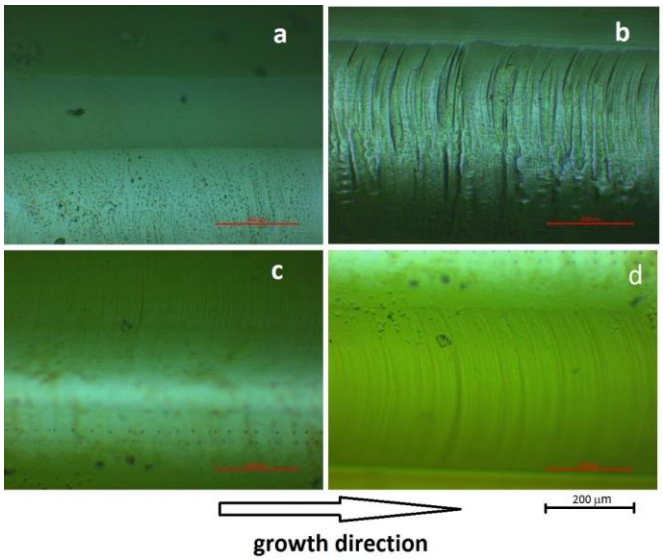

Fig. 1. Microscopic photos of LuAG:Ce fiber surfaces with L_{att} = 104 cm (a), L_{att} = 5.5 cm (b), surfaces of transparent part of YAG:Ce (YCV30) with L_{att} = 17.5 cm (c), and tail part of the same fiber (d).

To evaluate the effect of Al deficiency, a series of YAG:Ce fibers (Fig. 2) was produced with the different amounts of Al_2O_3 excess in the melt over the $3Y_2O_3$:$5Al_2O_3$ stoichiometric composition. In the 5 fibers presented in Fig. 2 we gradually changed the Al excess in the melt over the stoichiometric ratio from 20 to 370 ppm (Table. 1, Fig. 2).

Table 1. Attenuation length in fibers grown from melt with different Al^{3+} excess.

Sample	Ce conc, ppm	Al excess, ppm	Overall L_{att}, cm	L_{att} of the transparent part, cm	Length of the transparent part, cm	L_{att} *(transparent part)/overall* L_{att}
YCV30	100	<20	17,4	16,5	22	1
YCV31	100	110	14,4	20,0	16	1.4
YCV32	100	160	16,3	20,3	18	1.2
YCV33	100	210	10,4	26,7	15	2.6
YCV36	100	370	6,0	21,8	11	3.6

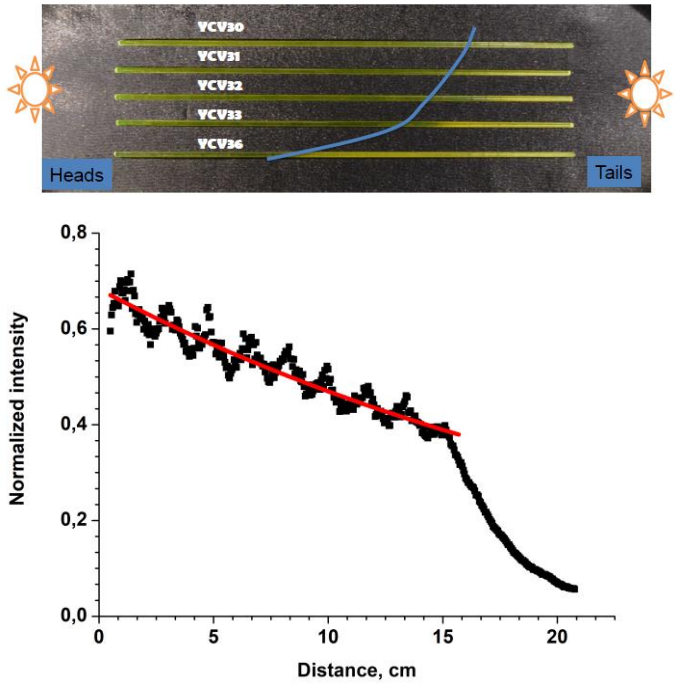

Fig. 2. Above: View of YAG:Ce fibers with increasing Al_2O_3 excess in the melt over stoichiometric composition (starting from the uppermost fiber) under the illumination from both sides by a daylight source. The blue line tentatively divides visually transparent and opaque parts of the fibers; Below: The dependence of luminescence intensity readout at the end of YCV33 on the position of excitation (at 470 nm) along the fiber length. The red line denotes the intensity fit by single exponential decay A_0 exp ($2x/L_{att}$), used at calculation of L_{att} in the transparent part of the fiber, where x is the distance from the place of excitation to the photodetector.

The fibers possess a distinct transparent part in the head (beginning), and the part with lot of inclusions in the tail (end). The L_{att} sharply decreases in the opaque part, as shown at the attenuation plot of YCV33. Under the illumination of fibers from both sides (Fig. 2) one may clearly observe how the transparent part length decreases with Al excess increase. While the L_{att} in the head parts was improved up to 20-27 cm, the overall L_{att} in 22 cm long fibers deteriorated with Al^{3+} excess introduction.

EPMA analysis of the fibers containing small and large Al excess shows that with the high 370 ppm excess of Al cerium segregates to the fiber tail (Fig. 3). XRD showed that opaque part contains Al_2O_3 phase inclusions. This means that Al^{3+} ions compete with Ce for substitution of Y^{3+} in dodecahedral sites in the garnet lattice (when antisite defects are formed) decreasing the Ce segregation coefficient. As at Ce concentration increase in garnet fibers the radial Ce segregation enforces [5], this calls surface roughness formed by melt meniscus instability. The latter is linked likely both to Ce accumulation, and Al_2O_3 phase inclusions.

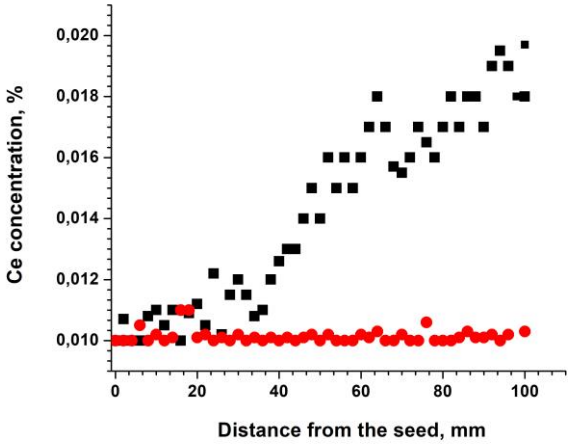

Fig. 3. Axial distribution of Ce along YAG:Ce fibers with the Ce content of 100 ppm and the Al excess of 15 ppm (red circles) and 370 ppm (black squares) in the melt.

The L_{att} dependences on Al^{3+} excess are shown in Fig. 4. One can see that the largest L_{att} of 27 cm is achieved at ~200 ppm Al excess, but the transparent part length decreases down to 15 cm. Thus, the optimal concentration interval of Al excess lies below 370 ppm and provides the attenuation length increase in the head part of the fibers. Al_2O_3 excess addition around 200 ppm compensates its evaporation from the melt, while larger Al_2O_3 concentrations lead to fiber quality degradation (Fig. 5). Therefore, Al_2O_3 evaporation is a notable factor determining the quantity of macrodefects in fibers grown by the μ-PD method providing a large melt surface/bulk ratio and flowing Ar atmosphere.

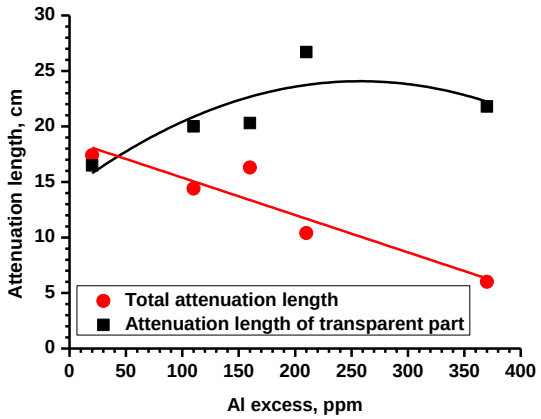

Fig. 4. Impact of Al excess on attenuation length of fibers.

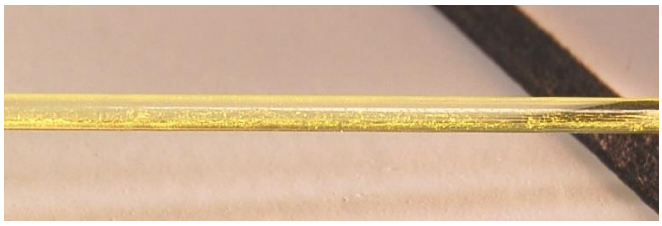

Fig. 5. Inclusions in the tail part of YCV36 fiber grown from the melt with the 370 ppm Al excess.

3.2. Improving stability of crystallization conditions

Assuming the melt meniscus instability in the end of growth as the main cause of fiber quality degradation, we focused on improving the stability of crystallization conditions. YAG:Ce fibers were crystallized from the melt meniscus of ~0.1 - 0.5 mm thickness. With fiber elongation and increase of heat removal through the fiber, the meniscus thickness tends to decrease (Fig. 6). The meniscus thickness of 0.1 – 0.2 mm is optimal, because the meniscus thickness over 0.2 mm leads to too high sensitivity of growth process to external vibrations. In meniscus with the thickness less than 0.1 mm the melt convection is weak, and admixtures segregated by the crystallization interface tend to accumulate in the periphery of the fiber. Also, when meniscus is thin, there is a danger of fiber contact with the capillary die calling fiber shape deterioration. Therefore, one should maintain the stable meniscus with the thickness of 0.1 – 0.2 mm. Under the stable heating power the meniscus thickness is determined by the two basic factors: vertical thermal gradient at the crystallization interface, and melt pressure inside the capillary die.

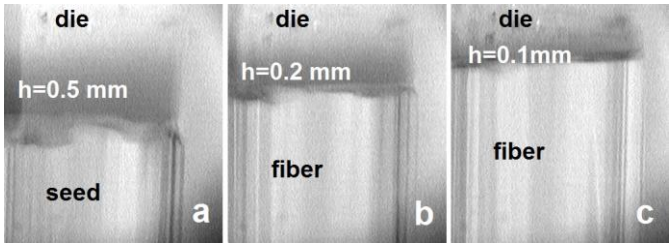

Fig. 6. View of YAG:Ce fiber crystallization process: fiber length 0.5 mm (a), 10 mm (b), 20 mm (c).

The vertical thermal gradient should be as large as possible to avoid melt supercooling in the meniscus. At the same time, melt pressure in the die should be large enough to maintain the meniscus thickness over 0.1 mm. Otherwise a low melt pressure in the die leads to YAG:Ce melt meniscus shape perturbations. This was not observed with LuAG:Ce, probably, because, the density of the latter is 1.5 times larger compared to YAG:Ce (6.7 vs. 4.55 g/cm^3 [10]). As the melt from the crucible is fed down to meniscus via the capillary die, the larger height of YAG:Ce melt column in the crucible is needed to maintain a large enough pressure in the capillary.

Growth under high thermal gradient requires the compensation of increasing heat removal during elongation of growing fiber. The overall heating power increase during the growth of 55 cm fibers was around 3%. The different power increase regimes were used, including continuous and stepwise power increase. The highest attenuation length of 38 cm was achieved with the stepwise power increase.

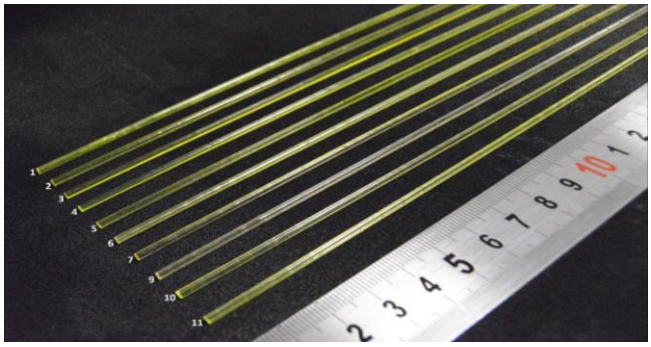

Fig. 7. Photo of a series of fibers grown under the optimized conditions. The fibers are numbered as YCD1-11, compositions and parameters of some of them are described in the text below.

Therefore, further experiments were carried out with twice larger initial amount of YAG:Ce melt in the crucible, and larger vertical thermal gradient at the crystallization interface. A series of 55 cm long fibers was grown under the optimized conditions (Fig. 7). Al excess in the 0-220 ppm range was introduced into the melt to adjust the optimal Al concentration. Discarding few centimeters long head and tail parts, two 22 cm long fibers were produced from each 55 cm long fiber. The fibers cut from the head parts were taken into further consideration, as the fibers cut from tail parts contained many visible inclusions. The L_{att} in the 22 cm long fibers increased up to 38 cm. According to Fig. 8, in such fibers grown under the optimized thermal conditions the optimal Al excess is around 120 ppm.

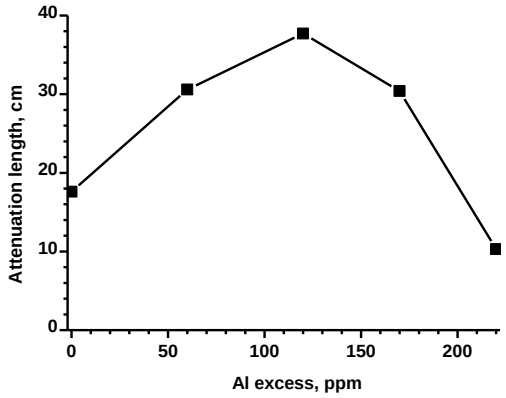

Fig. 8. Impact of Al excess on attenuation length of 22 cm long fibers grown under optimized conditions.

However, the Mg-codoped fibers did not follow this tendency. Adding 120 ppm of Al excess to the fibers codoped with 20-40 ppm of Mg strongly deteriorates the attenuation length from 35.7 cm to 4.2 cm (Table. 2).

Table 2. Attenuation length in 22 cm long YAG:Ce,Mg fibers grown from melt with different Al^{3+} excess over the stoichiometric compositions and varying Mg^{2+} concentration.

Name	$C(Al_{doped})$, Ppm	C(Mg), Ppm	Attenuation length, cm
YCD4	0	0	17.6
YCD10	0	20	24.3
YCD7	0	40	35.7
YCD5	170	0	30.4
YCD11	170	20	6.2
YCD9	170	40	4.2

3.3. Effect of thermal annealing of fibers

A drastic increase of L_{att} by up to 8 times achieved in LuAG:Ce fibers after thermal annealing in air [4] points at essential role of color centers related to oxygen vacancies in LuAG:Ce optical transmission. The same post-growth annealing of YAG:Ce fibers in air at 1200 °C did not give a reproducible positive result. The application of Arcal gas [3] with higher oxygen admixture concentration provided the L_{att} improvement just within 20 %. This points at inessential role of oxygen vacancies in degradation of optical transmittance in YAG:Ce. Meanwhile, for Mg-doped fibers the effect of thermal annealing is significant and enforces with Mg concentration (Fig. 9). In YAG:Ce,Mg fibers the L_{att} increased by up to 4 times. Higher oxygen vacancy concentration in Mg-codoped fibers is evidently caused by an excessive negative charge formed in the lattice at Y^{3+} substitution by divalent magnesium. This excessive charge can be compensated by Ce transfer into the tetravalent state and/or oxygen vacancy formation. Therefore, deterioration of L_{att} in as-grown YAG:Ce,Mg fibers is balanced by the strong increase of transmission after the thermal annealing in air. As the result, the maximal L_{att} achieved in YAG:Ce and YAG:Ce,Mg are about the same (38 cm vs. 36 cm).

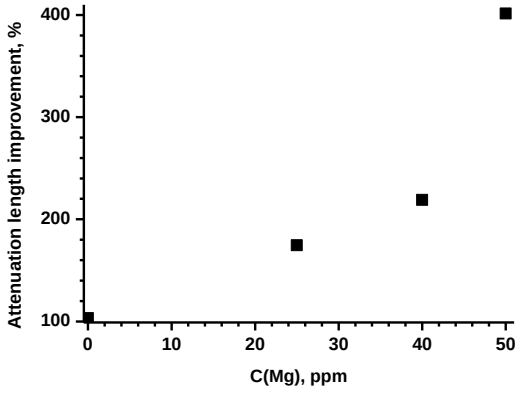

Fig. 9. Impact of air annealing at 1200 °C on YAG:Ce,Mg fibers attenuation length (100% corresponds to L_{att} before annealing) for different Mg concentrations.

3.4. Effect of Mg codoping on YAG:Ce scintillation decay time

Co-doping with Mg reduced the scintillation decay times of both fast and slow components, and increased the fast component contribution into the overall signal (Fig. 10, 11).

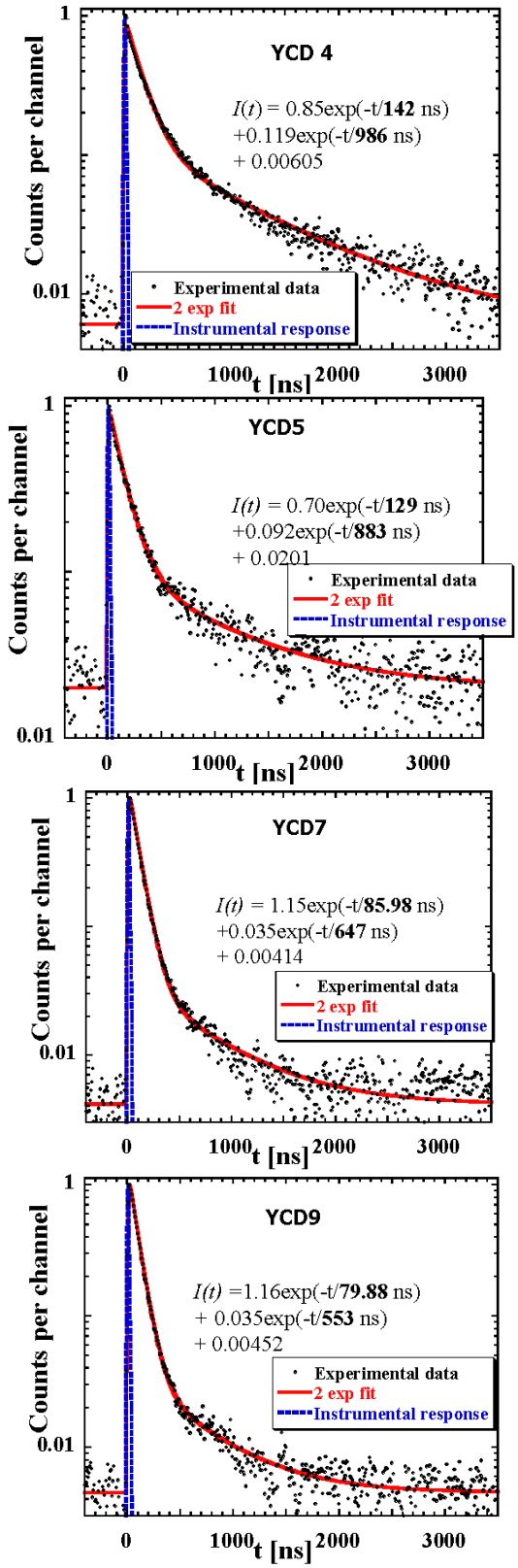

Fig. 10. Scintillation decay plots of some fibers (for reference see Table 2).

The shortest decay time was observed in the YCD9 fiber (≈80 ns), but it is still twice slower than the required value. The decay times clearly decrease with Mg concentration (Fig. 11) pointing that further increasing of Mg concentration above 40 ppm is necessary to reduce the decay time till the required amount. The decay times does not correlate with the absence/presence of Al excess certifying no impact of Al-related vacancies on carrier transport rate to Ce^{3+} luminescence centers. Meanwhile, Mg-codoped fibers should be grown without Al excess addition, as it sharply reduces the fiber attenuation length (see Table 2). The luminescence decay time decrease coincides well with other results on Ce,Mg codoped garnets, see for ex. [11] and our prior work [3]. As the decay time below 40 ns was achieved [11] in LuAG:Ce,Mg with heavy Mg doping with the ratio of $1Ce^{3+}$:$3Mg^{2+}$, there is a room for heavier Mg doping of YAG:Ce,Mg fibers.

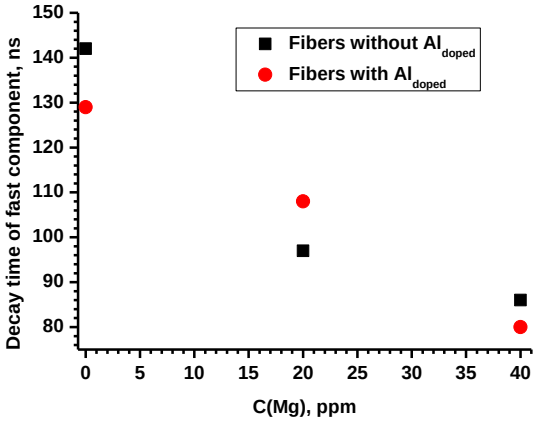

Fig. 11. Mg-codoping impact on decay time of YAG:Ce,Mg fibers.

Conclusions

The significant progress in transmission of YAG:Ce-based fibers has been achieved by adding of Al^{3+} excess into the melt and optimizing thermal conditions of crystallization by the μ-PD method. It was shown that LuAG:Ce fiber growth technology has to be modified to get YAG:Ce of comparable quality. Crystallization conditions of YAG:Ce and YAG:Ce,Mg growth were optimized by enforcing thermal gradient and increasing melt pressure in the capillary by adding more raw material into the crucible. As the result, the attenuation length of up to 38 cm was achieved in 22 cm long YAG:Ce fibers. Mg-codoped fibers did not show the tendency to L_{att} improvement with adding Al excess. However, optimization of thermal conditions and post-growth annealing provided the attenuation length enhancement up to 36 cm in YAG:Ce,Mg, which practically meets the requirements (40 cm) to detectors for future colliders. The scintillation decay time of the main fast component decreases from 142 to 80 ns with light Mg codoping. As in the fibers grown and annealed under the optimized conditions the Mg-codoping weakly affects the attenuation length, fibers with larger Mg concentrations should be grown further to decrease the scintillation decay time down to the required values.

Acknowledgements

The work was performed in the frame of Crystal Clear Collaboration and is supported by the Marie Skłodowska-Curie Research, Innovation Staff Exchange Project H2020-MSCA-RISE-2014 no.644260 “INTELUM”. Partial support of bilateral mobility project “Scintillation mechanisms in garnet- and perovskite-type crystals fabricated under different conditions” between Academies of Sciences of Ukraine and Czech Republic is also acknowledged.

Notes and references

1 A. Benaglia, M. Lucchini, K. Pauwels, C. Tully, T. Medvedeva, A. Heering, C. Dujardin, V. Kononets, K. Lebbou, N. Aubry, S. Faraj, G. Ferro, P. Lecoqa and E. Auffraya, *J. Instrum*., 2016, **11**, 05004.
2 M. T. Lucchini, K. Pauwels, K. Blazek, S. Ochesanu and E. Auffray, *IEEE Trans. Nucl. Sci.*, 2016, **63**, 586.
3 V. Kononets, K. Lebbou, O. Sidletskiy, Yu. Zorenko, M. Lucchini, K. Pauwels, and E. Auffray, pp. 114-128. In: Engineering of Scintillation Materials and Radiation Technologies, M. Korzhik and A. Gektin (eds.), Springer Proceedings in Physics 200, Springer International Publishing AG 2017, 339 p.
4 V. Kononets, E. Auffray, C. Dujardin, S.Gridin, F.Moretti, G.Patton, K.Pauwels, O. Sidletskiy, X.Xu, K.Lebbou, *J. Cryst. Growth*, 2016, **435**, 31.
5 X. Xu, K. Lebbou, F. Moretti, K. Pauwels, P. Lecoq, E. Auffray, C. Dujardin, *Acta Materialia*, 2014, **67**, 232.
6 Shiran, A. Gektin, K. Hubenko, V. Nesterkina, P. Arhipov, S. Tkachenko, O. Sidletskiy, *Func. Mater*., 2016, **22**, 299.
7 F. A. Selim, D. Solodovnikov, M. H. Weber, and K. G. Lynn, *Appl. Phys. Lett.*, 2007, **91**, 104105.
8 P. Arhipov, S Tkachenko, S Vasiukov, K Hubenko, Ia Gerasymov, V Baumer, A Puzan, P Mateychenko, K Lebbou, O Sidletskiy, *J. Cryst. Growth*, 2016, **449**, 104.
9 F. Cova, F. Moretti, M. Fasoli, N. Chiodini, K. Pauwels, E. Auffray, M.T. Lucchini, S. Baccaro, A. Cemmi, H. Bártová, A. Vedda, *Opt. Lett.*, 2018, **43(4)**, 903.
10 Scintillation Properties. S. Derenzo, M. Boswell, M. Weber, and K. Brennan (http://scintillator.lbl.gov/).
11 M. Nikl, K. Kamada, V. Babin, J. Pejchal, K. Pilarova, E. Mihokova, A. Beitlerova, K. Bartosiewicz, S. Kurosawa and A. Yoshikawa, *J. Cryst. Growth*, 2014, **14**, 4827.